

# Ultra-Wideband Imaging for Detection of Early-Stage Breast Cancer

X. Zhuge, M. Hajian, A.G. Yarovoy, L.P. Ligthart

*IRCTR Dept. Electrical Engineering,  
Delft University of Technology,  
Mekelweg 4, 2628 CD Delft, the Netherlands  
X.Zhuge@ewi.tudelft.nl*

**Abstract**—Ultra-wideband imaging for medical applications has been of interest for many years due to its high resolution and capability of detection and classification. In this paper, ultra-wideband near-field imaging is applied for detection of small malignant tumors inside breasts. Multiple antenna and focusing algorithm are used to form a spatial image of reflectivity, and to identify the presence and location of malignant lesions from their scattering signatures. The method is demonstrated by successful detection of a 2 mm diameter tumor in a three-dimensional numerical breast model.

## I. INTRODUCTION

Nowadays the standard diagnose for breast cancer is mammography, X-ray imaging of a compressed breast. Mammography has been proved to be quite sensitive to the presence of lesions in the breast. However, associations of this diagnose method with uncomfortable breast compression and unhealthy exposure to ionizing radiation may prevent patients from early-stage examination, which is the best and effective phase for medical treatment. These concerns provoke motivation for engineers to develop new breast imaging techniques.

Ultra-wideband imaging is an important alternative for mammography. The procedure is safe, simple and more comfortable for patients. The feasibility of UWB microwave imaging relies on two fundamental properties. Firstly, malignant tumors that have higher water content have higher dielectric properties than normal breast tissues, which have relatively lower water content. Therefore, strong scattering takes place at the boundary between normal tissue and lesions. Secondly, microwave attenuation in normal breast tissue is less than 4 dB/cm up to 10 GHz. This permits microwave devices to have enough sensitivity and dynamic range to detect early-stage tumors in this frequency band. By choosing an appropriate bandwidth, UWB technique can ensure images with high sensitivity and resolution.

Microwave imaging for breast cancer detection has been proposed and proven experimentally [1]-[7]. By using monostatic scanning system and MIST beamforming [1]-[3], malignant tumors are detectable by focusing backscattered signals while compensating for dispersive propagation through human body. In this paper, we proposed a multistatic UWB near-field imaging technique to detect tumors inside breasts. The proposed imaging technique uses a 2D

synthesized aperture array and a generalized near-field algorithm. This provides breast imaging with full 3D resolution and faster scanning. The imaging technique is subject to a number of assumptions. The dielectric properties of tissues are known (i.e., the complex permittivity as a function of frequency) from medical experiments. The normal breast tissue is supposed to be perfectly homogeneous except the region occupied by the malignant tumors.

This paper is organized as follows. Section II introduces the formulation of the proposed UWB imaging technique. Section III describes the three-dimensional numerical model and preliminary processing for further imaging. In section IV the numerical results of the imaging technique, based on the proposed method and MIST beamforming are presented and compared. Conclusions are given in section V.

## II. FORMULATION

The geometry of the setup is illustrated in Fig. 1, in which a transmit antenna illuminates the breast while an antenna array receives simultaneously the scattered field. The transmit/receive array mechanically moves around the breast to create a synthetic cylindrical aperture. Antennas are assumed to be point like and isotropic. The operational bandwidth is selected from 1 to 10 GHz. It is important to note that the observation distance will be within the near-field of the target. From imaging viewpoint, the target is the breast surface illuminated by the radar. Consequently, the image has to be focused using space-variant near-field focusing technique. Merging the breast in a tissue-mimicking material could be an option in order to minimize the distortion caused by complex refraction and also couple more power into the breast tissue.

### A. Scenario with tissue-mimicking dielectrics

Considering a point like tumor in the breast, its associated phase story will be defined by the electrical length of the two-way path travelling from the transmit antenna to the tumor, and scattering back to one of the receive antennas. When the breast is merged in a tissue-mimicking dielectric, we can assume that waves can pass breast boundary without refraction. This approach simplifies the estimation of propagation. Meanwhile, more power will be coupled into breasts, which increases the signal-to-interference-noise ratio (SINR) and eases the requirement of the dynamic range. The

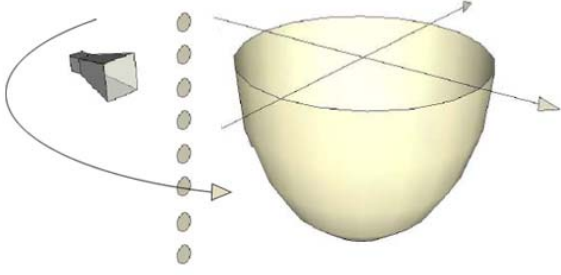


Fig. 1 Sketch of the scanning array and numerical breast model

electrical length of propagation is estimated as

$$R(\omega) = \sqrt{\epsilon_r(\omega)} [|\vec{r}_{Tx} - \vec{r}| + |\vec{r}_{Rx} - \vec{r}|] \quad (1)$$

where

$R$	frequency-dependent total electrical length from the transmit antenna to the tumor and back to the receive antenna
$\vec{r}$	location of tumor
$\vec{r}_{Tx}$ and $\vec{r}_{Rx}$	locations of transmit/receive antennas
$\epsilon_r(\omega)$	relative dielectric constant of the breast tissue

### B. Near-field image formation

Based on near-field focusing techniques, radar reflectivity at a point with coordinates  $(r, \varphi, z)$  can be estimated as follows:

$$I(r, \varphi, z) = \int_{\omega} \int_{z_{Rx}} \int_{\varphi_{Rx}} E(\omega, z_{Rx}, \varphi_{Rx}) F(\omega, z_{Rx}, \varphi_{Rx}, r, \varphi, z) d\varphi_{Rx} dz_{Rx} d\omega \quad (2)$$

where

$(r, \varphi, z)$	cylindrical coordinate of the target
$\omega$	frequency $\in [\omega_{min}, \omega_{max}]$
$E(\omega, z_{Rx}, \varphi_{Rx})$	frequency-domain backscattered data
$F(\omega, z_{Rx}, \varphi_{Rx}, r, \varphi, z)$	near-field focusing function

Specifically,  $F(\bullet)$  can be expressed as

$$F(\omega, z_{Rx}, \varphi_{Rx}, r, \varphi, z) = \exp \left[ j \left( \omega \frac{R(\omega)}{c} - \varphi_0 \right) \right] \quad (3)$$

where  $c$  is the speed of light and  $\varphi_0$  is the zero-phase reference point which, in turn, corresponds with the original probing pulse sent by the impulse radar system. Taking into consideration the frequency-dependence of breast tissues, dispersion is compensated, which leads to a better resolution.

The focusing function in (3) can be reformulated as  $F(\omega, z_{Rx}, r, \varphi - \varphi_{Rx}, z)$ . Then (2) becomes a convolution between the backscattered fields and focusing function over the azimuth. This integration can be efficiently implemented by fast Fourier transform (FFT) as complex product in the wavenumber domain [8]. Then (2) becomes

$$I = \text{IFFT}_{\varphi} \left\{ \sum_{\omega} \sum_{z_{Rx}} \text{FFT}_{\varphi} [E(\omega, z_{Rx}, \varphi_{Rx})] \text{FFT}_{\varphi} [F(\omega, z_{Rx}, r, \varphi, z)] \right\} \quad (4)$$

### C. Microwave imaging via space-time beamforming (MIST)

By requiring the signals to pass with unit gain and linear phase shift, MIST beamforming handles the frequency dependent propagation effects by designing the beamformer weight over channels in each frequency [3]

$$I(\omega) \sum_{i=1}^M \tilde{S}_{ii}(\vec{r}, \omega) \cdot W_i^*(\omega) = e^{-j\omega\tau_0} \quad (5)$$

where

$I(\omega)$	DFT of the transmitted signal
$\tilde{S}_{ii}(\vec{r}, \omega)$	monostatic frequency response for $i^{th}$ channel
$M$	total number of antennas
$\tau_0$	average time delay
$W_i(\omega)$	beamformer weight for $i^{th}$ channel

By solving a penalized least square problem, the beamformer weight can be expressed as [3]

$$W_i(\omega) = \frac{\tilde{S}_{ii}(\vec{r}, \omega) e^{j\omega\tau_0}}{|\tilde{S}_{ii}(\vec{r}, \omega)| (1 + \sum_{j=1}^M |\tilde{S}_{jj}(\vec{r}, \omega)|)} \quad (6)$$

Amplitude correction is included in this algorithm in order to compensate the propagation loss. This helps to increase the dynamic range. In the meantime, an accurate estimation of the complex permittivity is needed. MIST beamforming can be extended for multistatic systems by simply adjusting the transfer function.

### D. Estimation of dispersive dielectric properties

The frequency dependence of the dielectric constant,  $\epsilon_r(\omega)$ , over the bandwidth of the proposed impulse system can be modeled by using the first order Debye dispersion function in the following form [9]:

$$\epsilon(\omega) = \epsilon_0 \left( \epsilon_{\infty} + \frac{\epsilon_s - \epsilon_{\infty}}{1 + j\omega\tau} \right) \quad (7)$$

which describes a dielectric's relaxation process by determining the relaxation time,  $\tau$ , and the epsilon static values,  $\epsilon_s$  and  $\epsilon_{\infty}$ . The Debye model parameters are selected here according to the published data for breast tissues [9]:

- skin	$\epsilon_s = 36, \epsilon_{\infty} = 4, \tau = 7.23\text{ps}$
- normal tissue	$\epsilon_s = 10, \epsilon_{\infty} = 7, \tau = 7.0\text{ps}$
- malignant	$\epsilon_s = 54, \epsilon_{\infty} = 4, \tau = 7.0\text{ps}$

## III. EM MODEL AND DATA PRE-PROCESSING

The challenge in the research of breast cancer detection is to build a numerical model that can approximate the complex dielectric profile inside the breast under acceptable simulation time and computational cost. In this paper, a finite integration (FIT) model shown in Fig. 1 is built by using the commercial software CST. We assume a configuration where a linear array is placed close to the breast which is naturally extending

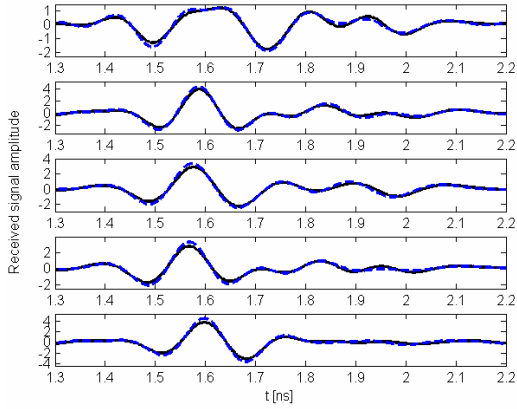


Fig. 2 Backscattered signal after skin artifact removal by average subtraction (solid) and adaptive artifact removal algorithm (dashed)

through a hole on the examination table when the patient orients in a prone position. The three-dimensional numerical breast model has a realistic ellipsoidal contour with 10 cm width and is merged in a tissue-mimicking material that matches the properties of breast tissue at the central frequency (5.5 GHz). It has a 2 mm skin layer and a spherical tumor with 2 mm diameter.

The dispersive dielectric properties of skin, normal and malignant breast tissue are also included in the FIT model. The frequency dependence of dielectric properties are incorporated into the simulation by using the Debye model as described in (7).

Pre-processing was applied before the formation of images. Due to finite bandwidth and also the possible close distance between tumor and skin layer, skin reflections and tumor responses are not separated in time in the received signals. Because the reflections from skin-breast layer have much larger magnitude than tumor reflections, it must be removed before applying the imaging algorithm. A common approach to remove the skin reflection is average subtraction. This method assumes the received skin reflections are the same among channels. It works well in ideal situation, but is not valid for complex scenarios. An adaptive artifact removal algorithm is proposed in [2]. Based on the fact that the skin reflections among channels are similar but not identical, this algorithm estimates the artifact in each channel as a filtered combination of the signal in all the other channels. Therefore, this approach is able to handle minor variations of skin reflections among channels. Due to the use of single transmit antenna, the signal strength is non-uniformly distributed over the array elements. Therefore, the artifact removal algorithm needs to be applied among signals from the same array element over the azimuth scan. A comparison of signals after skin artifact removal by both methods is illustrated in Fig. 2. The tumor responses are well preserved by both approaches and match with each other when there are no skin variations and heterogeneity.

#### IV. RESULTS

After pre-processing, the proposed imaging algorithm was

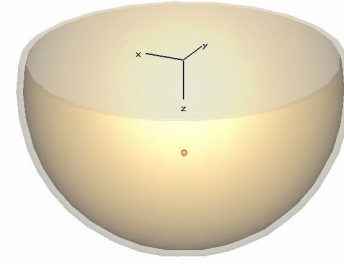


Fig. 3. Numerical breast phantom with a 2 mm diameter malignant tumor centered at (0 cm, 0 cm, 3 cm).

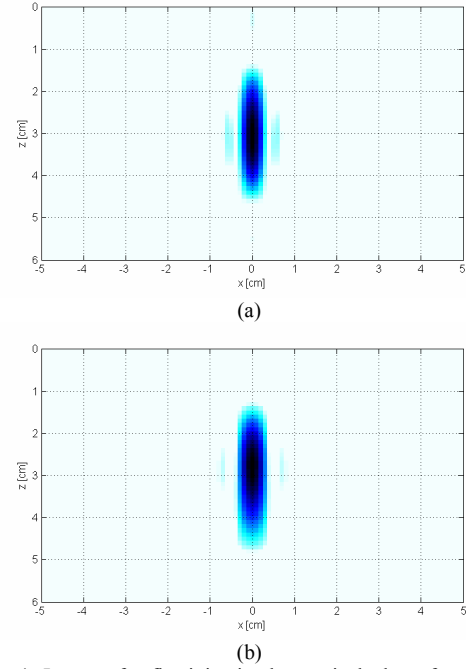


Fig. 4. Image of reflectivity in the vertical plane from (a) generalized near-field imaging algorithm (b) MIST beamforming

applied for validation. The time-domain signals were first transformed to frequency domain. Then the reference phase over frequency was obtained by recording the transmitted signal and was subtracted from the frequency domain data set. A 3D image within the volume of the phantom was reconstructed through (2) with a 1 mm pixel resolution. The synthetic aperture was cylindrical with 12 azimuth angles and a radius of 6 cm.

We performed the validation in two steps. At first, in order to compare the focusing capability of the proposed algorithm and MIST beamforming, the models with and without tumor were both simulated and the tumor response was obtained by subtraction so that the imaging will not be affected by clutter. A 2 mm diameter tumor was placed in the centre and kept 3 cm distance from the top of the model as shown in Fig. 3. Fig. 4 shows the two-dimensional images obtained in the vertical cutting plane. The dynamic range shown in these images is 15 dB. It can be seen that the peak value corresponds with

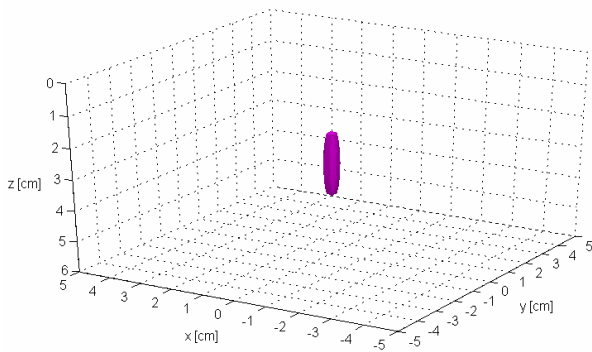


Fig. 5. Three-dimensional image of reflectivity for the model in Fig. 3 with a 2 mm diameter malignant tumor centered at (0 cm, 0 cm, 3 cm).

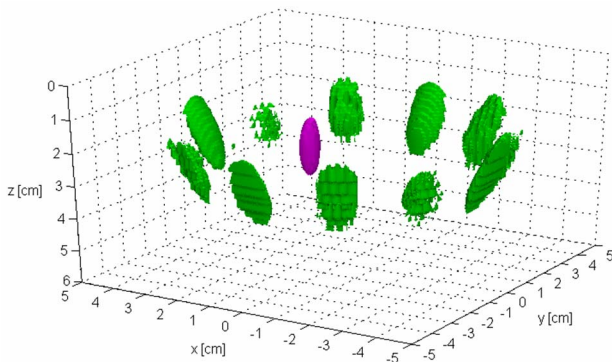


Fig. 6 Three-dimensional image of reflectivity for the model similar to that of Fig. 5 with a 2 mm diameter malignant tumor centered at (1 cm, 0 cm, 2.5 cm).

the actual position of the tumor. Both algorithms provide similar down-range and cross-range resolution. This implies that distortion in the received signals caused by the refraction and dispersion of the waves are successfully corrected by both algorithms. The shape of tumor in the 3D image is ellipsoidal instead of its real spherical shape (Fig. 5). This is due to the limited extension of array in the vertical direction, which leads to coarser cross-range resolution than the down-range. Employing a spherical aperture instead of cylindrical is recommended in practical situation in order to trade cross-range aperture with down-range bandwidth. The inclusion of amplitude correction may increase the level of sidelobe associated with clutter. Further investigations are needed to check the possible degradation of algorithms caused by the heterogeneity of the breast tissues.

Then the tumor was replaced in the same model as Fig. 3 but with offset at position (1 cm, 0 cm, 2.5 cm). This time the adaptive artifact removal algorithm was applied to obtain the signals for imaging. The corresponding three-dimensional image is illustrated in Fig. 6. The tumor is clearly indicated at the correct location. Clutter appear around the surface of the

breast model in front of the locations of array. This is caused by the residuals of skin reflection left by the adaptive artifact removal algorithm. Detecting tumors close to the skin in the presence of these residuals will be challenging.

Using a 2.68GHz workstation, the computation time needed to obtain the 3D volume shown in Fig. 6 (61×51×360 pixels) is about 20 minutes for the whole imaging process. By recording the focusing function in (3) and reusing it, the computation efficiency can be further improved.

## V. CONCLUSIONS

In this paper, a multistatic UWB near-field imaging algorithm for breast cancer detection is introduced. Demonstration of this method is carried out by successfully detecting a 2 mm diameter tumor in a three-dimensional dispersive breast model. The results show that the proposed algorithm can effectively minimize the distortion caused by complex refraction and dispersive dielectric properties and drastically reduce the computing time.

## REFERENCES

- [1] X. Li, E. J. Bond, B. D. Van Veen, and S. C. Hagness, "An overview of ultrawideband microwave imaging via space-time beamforming for early-stage breast cancer detection," *IEEE Antennas and Propagation Magazine*, vol. 47, no. 1, pp. 19-34, Feb. 2005.
- [2] E. J. Bond, X. Li, S. C. Hagness, and B. D. Van Veen, "Microwave imaging via space-time beamforming for early detection of breast cancer," *IEEE Trans. Antennas and Propagation*, vol. 51, no. 8, pp. 1690-1705, August 2003.
- [3] S. K. Davis, E. J. Bond, X. Li, S. C. Hagness, and B. D. Van Veen, "Microwave imaging via space-time beamforming for early detection of breast cancer: Beamformer design in the frequency domain," *Journal of Electromagnetic Waves and Applications*, vol. 17, no. 2, pp. 357-381, 2003.
- [4] R. Nilavalan, A. Gbedemah, I. J. Craddock, X. Li and S. C. Hagness, "Numerical investigation of breast tumor detection using multi-static radar," *Electronics Letters*, vol. 39, no. 25, pp. 1787-1788, Dec. 11, 2003.
- [5] E. Fear, X. Li, S. C. Hagness, and M. Stuchly, "Confocal microwave imaging for breast cancer detection: Localization of tumors in three dimensions," *IEEE Trans. Biomed. Eng.*, vol. 49, no. 8, pp. 812-822, August 2002.
- [6] Benjamin, R.; Craddock, I.J.; Leendertz, J.; Nilavalan, R.; Preece, A., "Experimental investigation of real aperture synthetically organised radar for breast cancer detection," *Antennas and Propagation Society International Symposium, 2005 IEEE*, Volume 1B, 2005 Page(s):179 - 182 vol. 1B
- [7] Nilavalan, R.; Leendertz, J.; Craddock, I.J.; Preece, A.; Benjamin, R., "Numerical analysis of microwave detection of breast tumours using synthetic focussing techniques," *Antennas and Propagation Society International Symposium, 2004. IEEE*, Volume 3, 20-25 June 2004 Page(s):2440 - 2443 Vol.3
- [8] Joaquim Fortuny and Alois J. Sieber, "Fast Algorithm for a Near-Field Synthetic Aperture Radar Processor," *IEEE Trans. Antennas and Propagation*, vol. 42, pp. 1458-1460, October 1994.
- [9] E. Zastrow, S. K. Davis, and S. C. Hagness, "Safety assessment of breast cancer detection via ultrawideband microwave radar operating in pulsed-radiation mode," *Microwave and Optical Technology Letters*, vol. 49, no. 1, pp. 221-225, Jan. 2007.